Applied Numerical Modeling in Geomechanics – 2020 – Billaux, Hazzard, Nelson & Schöpfer (eds.) Paper: 03-04

Application of *PFC3D* to study railroad ballast breakage response under train loading

B. Dahal[1], D. Mishra[2] & D. Potyondy[3]
[1] *Bailey Engineering, Inc., Boise, ID, USA*
[2] *Department of Civil and Environmental Engineering, Oklahoma State University, Stillwater, OK, USA*
[3] *Itasca Consulting Group, Inc., Minneapolis, MN, USA*

1 INTRODUCTION

In a ballasted railroad track system, the ballast layer performs important functions like resisting forces from trains, distributing train-induced pressures to the subgrade at acceptable stress levels, and facilitating free drain conditions (Selig & Waters 1994). Under train-induced repeated loading, these angular ballast particles (often as large as 63 mm) undergo significant amounts of breakage resulting in ballast layer fouling which adversely affects the shear strength characteristics, causes an increase in vertical settlements, and rapidly deteriorates the drainage conditions. About 76% of the fouling fines have been reported to originate from ballast breakage (Selig & Waters 1994), and it has been reported that the maintenance costs associated with the ballast layer performance are also very high (Lobo-Guerrero & Vallejo 2006).

Several researchers have studied the effects of ballast breakage on ballast layer performance under repeated loading; studies have been conducted in the laboratory (Indraratna et al. 1998) and using numerical modeling methods (Lobo-Guerrero & Vallejo 2006). Even though the laboratory setting can simulate actual field conditions, numerical methods like the Distinct Element Method (DEM) can provide a complete picture of the particle breakage phenomenon (Indraratna et al. 1998), because DEM can be used to study details such as breakage initiation, evolution, etc.

To understand the significance of ballast breakage considerations on permanent deformation (PD) behavior of railroad ballast under repeated loading, a study using *PFC3D* (Itasca 2018) was carried out. First, the study used unbreakable ellipsoids as representative ballast particles to establish preliminary modeling parameters. Subsequently, the model was improved by considering breakable ballast particles modeled as agglomerates of spheres to approximate the polyhedral shapes of ballast particles. Bond strength values (primarily governing the particle breakage) assigned to the ballast agglomerates were modified from the literature (Indraratna et al. 2010a).

2 DESIGN AND ANALYSIS

First, to replicate the geometry of a polyhedral ballast particle, this study utilized a cost-effective imaging technique. Smartphone cameras were used to capture high-resolution images of the ballast particles that were subsequently digitized using the Autodesk Recap Software (Autodesk 2018). These digitized images were imported into the *PFC* model to define templates for individual ballast particles. Figure 1a shows one such image of a ballast particle; Figure 1b shows a digitized version of the same image using Autodesk Recap Software. Three different ballast shapes were thus digitized to be used in subsequent *PFC* models.

To obtain particle crushing strength values and appropriate ballast bond strength parameters, selected ballast particles were subjected to Single Particle Crushing Tests (SPCTs) in the laboratory. The force-

displacement plots obtained from these tests were used to calibrate diametral compression (DC) tests using the material modeling support package in *PFC* (Potyondy 2018). Slight modifications were implemented into this package to ensure an accurate representation of the laboratory test setup. Detailed information regarding the SPCT and the corresponding calibration efforts will be published in future manuscripts. Figures 1c and 1d show photographs of the SPCT test set-up and the crushed ballast particle after the testing, respectively. Figure 1e shows the SPCT test being simulated in *PFC* using the diametral-compression capability. Figure 1f shows the same model with the particle breakage path highlighted using red disks to show the broken bonds. Bond strengths assigned within the model were adjusted until the simulated load-displacement curve closely matched the laboratory-generated curve. The calibrated model parameters are listed in Table 1.

Once the ballast shapes were created and calibrated using the SPCT test results, a specimen box of size 600 mm × 600 mm × 300 mm was created using *PFC3D* to represent a scaled version of a railroad ballast layer. Ballast particles were distributed in the box following the particle size distribution reported by Dahal et al. (2018). Each size distribution comprised equal proportions of ballast particles conforming to the three different ballast shapes. Note that the three different particles shapes were generated as agglomerates of different numbers of smaller spheres (12, 7, and 12). These numbers were smaller than the number of spheres used to simulate the SPCT. This was necessary because using a significantly larger number of spheres to generate each ballast particle in the larger ballast model leads to unreasonable computational times. Nevertheless, the bond strengths assigned within each ballast agglomerate in the larger model exactly matched those established through the SPCT simulations.

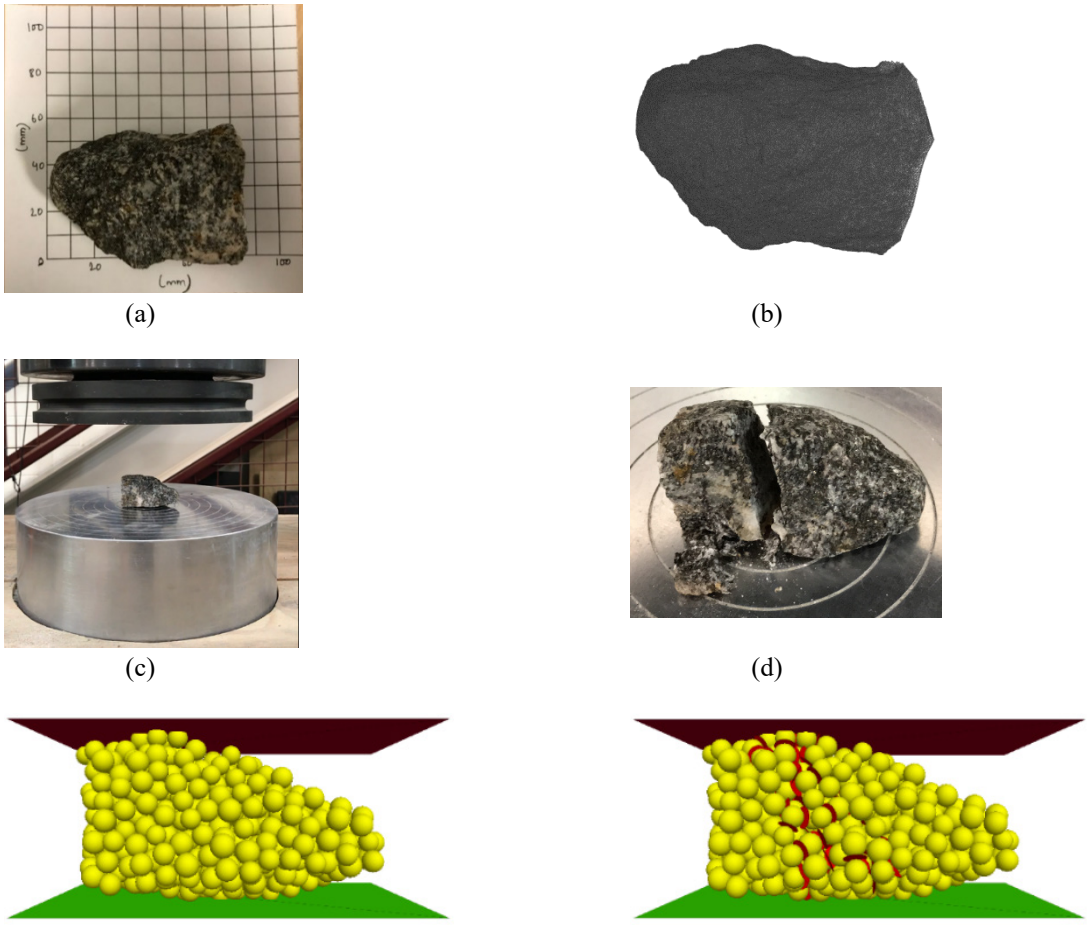

Figure 1. a) Photograph of ballast particle captured using smartphone; b) same photograph digitized using the Autodesk Recap software; c) laboratory test setup for conducting the Single Particle Crushing Test (SPCT); d) crushed ballast particle after completion of the SPCT; e) *PFC* model of the SPCT; and f) simulated ballast particle breakage in *PFC* (the red disks show broken bonds).

Table 1. Model parameters used in simulation.

General Parameters			Parallel Bond (PB) Parameters		
Specimen size	:	L=600; W=600; H=300	PB Normal Stiffness, $\overline{k_n}$	=	1.48×10^{11} N/m^3
Density	:	2610 kg/m^3	PB Shear Stiffness, $\overline{k_s}$	=	7.58×10^{10} N/m^3
Wall Effective Modulus	:	3 GPa	PB Normal Strength, σ	=	3.83×10^{6} N/m^2
Ballast Effective Modulus	:	0.833 GPa	PB Shear Strength, τ	=	1.57×10^{7} N/m^2
Poisson's Ratio	:	0.2	PB Radius Multiplier, $\bar{\lambda}$	=	1
Friction	:	0.5			
Ballast-Ballast Contact Model	:	Hill Contact Model			
Ballast-Wall Contact Model	:	Linear Contact Model			

The ballast particles are first modeled as unbreakable clumps. They were generated in the specimen box and were allowed to settle under gravity. Then a material pressure of 20 kPa (range 10-60 kPa) was applied to the ballast layer from the enclosing walls of the specimen box using the servo mechanism of *PFC* to account for the initial confinement pressures provided by crossties, shoulder and crib ballasts (Indratana et al. 2010b). After this stage, a cyclic loading with an amplitude of 187 kPa and a mean stress of 232 kPa was applied to the ballast specimen via the top wall of the specimen box. All ballast particles were modeled as unbreakable during this stage.

To simulate the ballast breakage mechanism, the unbreakable ballast clumps were deleted and replaced with clusters of spheres with the same radii at the same positions as each clump pebble. These sphere clusters were bonded using the linear parallel bond contact model. The bonds in this model eventually undergo breakage when forces (shear/tensile) at contact points exceed pre-defined strength values. Upon breakage, the Hill contact model (Potyondy 2016) was applied to every new ballast-ballast contact. The Hill contact model provides the behavior of two locally elastic spheres via Hertz-Mindlin springs. The bond parameters used in this simulation are listed in Table 1. After this step, cyclic loading was applied to the ballast layer via the top wall of the specimen box and the stress-strain response of the ballast layer was measured. Detailed information about the model generation, applied cyclic loading and breakage behavior can be found in Dahal et al. (2018).

3 RESULTS AND DISCUSSION

Figure 2a shows the evolution of vertical axial strain with the number of load cycles. As seen from the figure, there is an initial bulging of approximately 8.39%. This can be attributed to the overlap between cluster of bonded spheres forming the ballasts shapes. Once there is a breakage in the specimen, forces associated with ballast particle overlaps result in the instant bulging of the ballast layer. After this energy is released, there is sudden increase in vertical axial strain with initial load cycles. After the initial cycle, axial strain is found to increase in a steady manner and towards the end of 50 load cycles, the permanent axial strain is found to have stabilized. Figure 2b shows the plot of applied cyclic stress versus vertical axial strain for 50 load cycles. Initially, the axial strain is negative which corresponds to bulging of the specimen. After bulging is over, the axial strain accumulation after the first few load cycles is significantly higher than under successive load cycles (about 5% permanent axial strain). In this plot, the spikes in stress-strain response during the first few load cycles can be attributed to particle breakage. The ballast stress-strain response is elastic towards the end of 50 load cycles, showing a near-complete hysteretic behavior. This demonstrates the resilient behavior of the ballast layer after it has been subjected to a large number of load cycles.

The number of linear parallel bonds before and after 50 load cycles were 56652 and 1369, respectively; a total of 55283 bonds were broken upon cyclic loading. Most of these bond breakages occurred during the initial load cycles after which broken ballast particles rearranged themselves in the void spaces. This clearly illustrates the fact that particle breakage is the major source of permanent axial strain in the ballast layer.

To compare the results obtained from the ballast layer comprising polyhedral ballast shapes with the ballast layer comprising ellipsoid shapes (as used in Dahal et al., 2018), the exact simulation was repeated using ellipsoid ballast shapes. Note that both shapes were modeled using agglomerates of spheres. Figure 2c shows the evolution of permanent strain accumulation with number of load cycles, and Figure 2d shows the plot of change in particle size distribution before and after cyclic load for polyhedral and ellipsoid ballast shapes. After the initial bulging for both ballast shapes, the accumulated permanent axial strain at the end of 50 load cycles was found to be 5.09% and 3.36% for polyhedral and ellipsoid ballast shapes, respectively. The accumulated permanent axial strain for the polyhedral ballast layer was approximately 51.5% more than for the ellipsoid ballast layer. Moreover, comparing the shift in particle size distribution before and after cyclic loading for two different particles shapes, the polyhedral ballast particles underwent a significantly higher degree of breakage than the ellipsoid ballast particles.

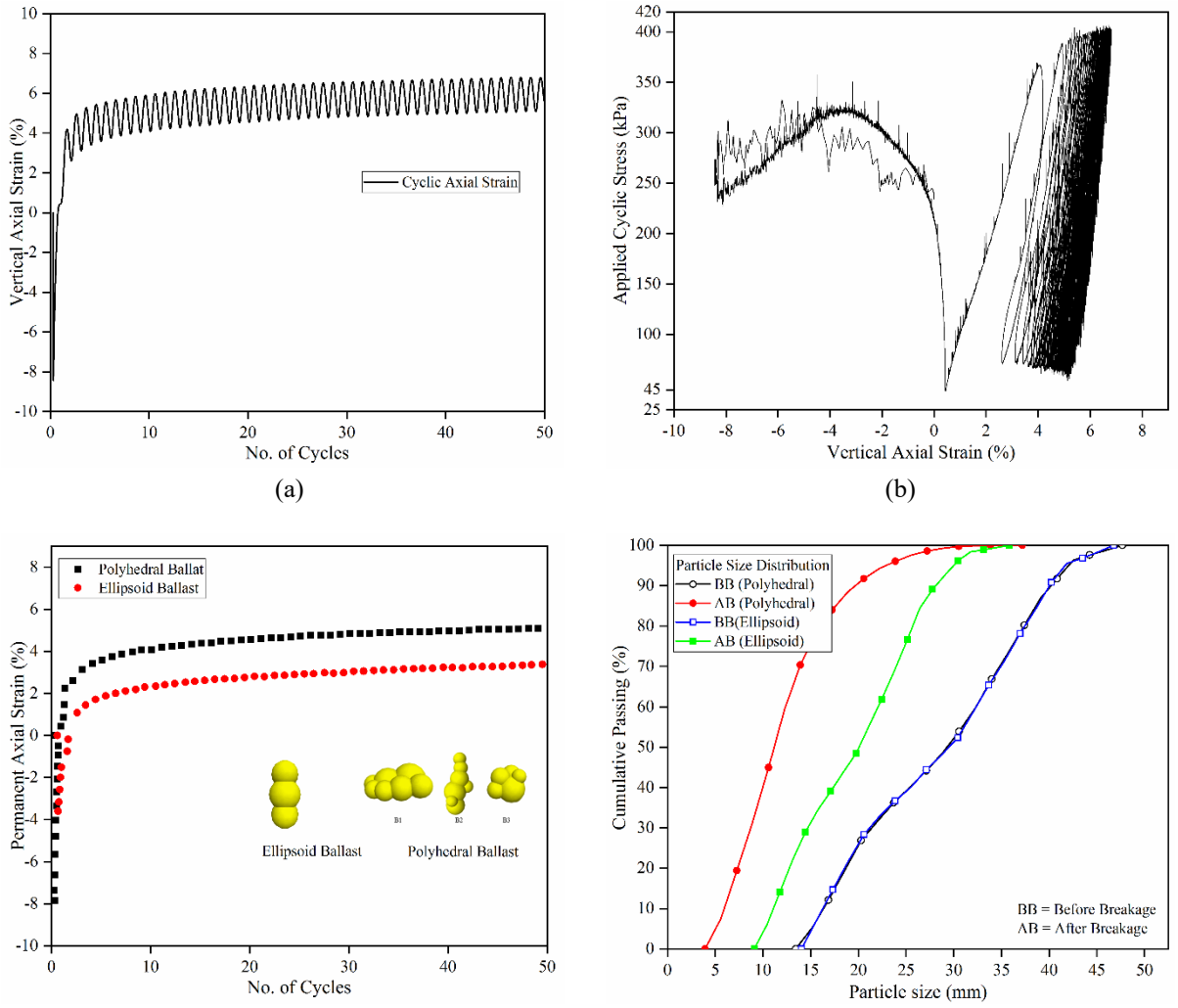

Figure 2. a) Vertical axial strain in the ballast layer vs. number of load cycles; and b) applied stress vs. vertical axial strain for polyhedral ballast shapes. c) Permanent strain accumulation in the vertical direction vs. number of load cycles; and d) change in particle size distribution before and after cyclic load application for both polyhedral and ellipsoid ballast shapes.

4 CONCLUSIONS

Through simulation of railroad ballast layer behavior under cyclic loading, it was observed that particle breakage during the initial load cycles plays a significant role in governing the overall permanent

deformation accumulation. As the number of particle breakages under subsequent load cycles decreases significantly, the rate of permanent axial strain is also reduced.

Comparing the results for different ballast shapes, it was observed that accurate representation of ballast particles shapes can significantly affect the simulation results. At this point, it should be noted that differences in particle shape did not have a significant effect on total permanent axial strain for non-breakable particles, as reported in Dahal et al. (2018). However, when particle breakage was taken into consideration, particle shape played a significant role in governing total permanent axial strain under loading.

REFERENCES

Autodesk Inc. 2018. From *https://www.autodesk.com/products/recap/overview* <June 10, 2019>.

Dahal, B., Mahmud, S.M. & Mishra, D. 2018. Simulating ballast breakage under repeated loading using the discrete element method. *Joint Rail Conference 2018 April 18-20, Pittsburgh PA*.

Indraratna, B., Ionescu, D. & Christie, D. 1998. Shear behavior of railway ballast based on large-scale triaxial tests. *ASCE J. Geotechn. Geoenviron. Eng*. 124(5), 439-449.

Indraratna, B., Thakur, P.K. & Vinod, J.S. 2010a. Experimental and numerical study of railway ballast behavior under cyclic loading. *Int. J. Geomech.* 10(4), 136–144.

Itasca Consulting Group, Inc. 2018. *PFC3D – Particle Flow Code in 3 Dimensions, Ver. 6.0*. Minneapolis: Itasca.